Advanced Nonlinear System Identification for Modal Interactions in Nonlinear Structures: A Review

K. J. Moore, A. Mojahed, M. Kurt, M. Eriten, D. M. McFarland, L. A. Bergman and A. F. Vakakis

Abstract In this work, we review a recently developed method for the characterization and identification of strongly nonlinear dynamical systems, including the detection of strongly nonlinear modal interactions, directly from transient response data. The method synergistically combines the proper orthogonal decomposition and the Rayleigh quotient to create estimated frequency-energy plots (FEPs) that capture the rich and interesting nonlinear dynamical interactions. The method is first applied to the experimentally measured response of a cantilever beam with a local, smooth nonlinearity. In this application, the estimated FEP reveals the presence of nonsmooth perturbations that connect different nonlinear normal modes (NNMs) of the system. The wavelet-bounded empirical mode decomposition and slow-flow analysis are used to demonstrate that the nonsmooth perturbations correspond to strongly nonlinear internal resonances between two NNMs. In the second example, the method is applied to the experimentally measured response of a cantilever beam

K. J. Moore (✉) · A. Mojahed · D. M. McFarland · L. A. Bergman · A. F. Vakakis
University of Illinois, Urbana, IL 61801, USA
e-mail: kmoore14@illinois.edu

A. Mojahed
e-mail: mojahed2@illinois.edu

D. M. McFarland
e-mail: dmmcf@illinois.edu

L. A. Bergman
e-mail: lbergman@illinois.edu

A. F. Vakakis
e-mail: avakakis@illinois.edu

M. Kurt
Stevens Institute of Technology, Hoboken, NJ 07030, USA
e-mail: mkurt@stevens.edu

M. Eriten
University of Wisconsin-Madison, Madison, WI 53706, USA
e-mail: eriten@engr.wisc.edu

D. M. McFarland
Zhejiang University of Technology, Hangzhou 310014, Zheijiang, China

I. V. Andrianov et al. (eds.), *Problems of Nonlinear Mechanics and Physics of Materials*, Advanced Structured Materials 94,
https://doi.org/10.1007/978-3-319-92234-8_7

with a local, nonlinear attachment in the form of a nonlinear energy sink (NES). An estimated frequency-displacement plot for the NES is created, and an optimization routine is then used to identify the unknown parameters for a given model of the nonlinearity. Ultimately, the method is conceptually and computationally simple compared to traditional methods while providing significant insight into the nonlinear physics governing dynamical systems with strong, local nonlinearity directly from measured time series data.

1 Introduction

Modal analysis, system identification and reduced-order modeling have been thoroughly studied in [5, 8, 28]. Nonlinear system identification (NSI) methods for nonlinear dynamical systems [15, 26], including the method of proper orthogonal decomposition (POD), [6, 13, 14, 16, 22] and a new promising technique for nonlinear system identification [31], which involves employing empirical mode decomposition (EMD) [7, 10, 11, 33], that operates under the assumption that measured time series can be decomposed into a finite set of harmonic components in the form of fast, nearly monochromatic oscillations that are modulated by slowly varying amplitudes. Using these NSI techniques, [17] showed that strong nonlinearities can lead to strongly nonlinear beat phenomena, which are the result of strongly nonlinear modal interactions, i.e. internal resonances (IRs) which occur between the nonlinear normal modes of the system.

Nonlinear normal modes (NNMs) are defined to be time-periodic oscillations, which one may regard as the nonlinear extensions of the linear vibrational normal modes [30]. While there are no modal interactions, the NNMs are synchronous, time-periodic oscillations; in contrast, in the case that IRs happen (which results in nonlinear energy exchange between modes), mode mixing is realized. In this case, non-synchronous oscillations with more than one participating NNM occur which cause scale mixing in the nonlinear dynamics that makes scale separation impossible. IRs depend highly on the total energy of the system and the necessary condition for them to occur is that the frequency ratio of the NNMs is a rational number. Also, IRs take place at different energy levels due to the fact that lower NNMs are affected at lower energy levels while higher NNMs are not affected as much. IRs have been shown to cause energy localization as in targeted energy transfer [29, 30], which lead to significantly altered stress distributions that can result in component failures [4], along with triggering bifurcations in the dynamics that change the stability of NNMs [1].

Utilizing POD to extract proper orthogonal modes (POMs), which represent the participating NNMs, and computing the Rayleigh quotient (RQ) using the POMs as trial vectors, [9] generalized the results described in [17]. By plotting the resulting RQs as functions of energy in the form of a frequency-energy plot (FEP) [29], it was revealed that the dynamics of the nonlinear system can be divided into three distinctive regimes. Of these, two are linear–in the low and high energy limits–

and are connected by the third regime,a strongly nonlinear transition regime. The duration of this nonlinear transition regime has been found to increase with increasing frequency. These regimes are different for each NNM because each modal response depends on the system energy. Additionally, by looking at the the RQ-FEP curves, one can see that there exist a number of non-smooth perturbations (spikes) which appeared to be the result of NNMs mixing due to occurrence of IRs.

The study performed by [23] on two comparable cantilever beams, each with strong, local nonlinearity led, to a physical interpretation of these spikes and substantiated the claim that these spikes represent modal interactions in the dynamics of stronlgy nonlinear systems. In order to investigate the physics of the spikes, POMs corresponding to RQs off and on the spikes were examined. The POMs computed off the spikes were found to correspond to periodic solutions of the non-interacting NNMs, while on the spikes the POMs of interacting NNMs were found to be similar and corresponded to the mixed periodic solutions of the NNMs during an IR. Furthermore, in the displacement responses for points on and off the spikes the presence of slow-flow dynamics [18, 20, 21, 31], which occurs as result of IRs, was investigated by means of the wavelet-bounded empirical mode decomposition [25]. The aforementioned analysis showed that only the responses corresponding to points on the spikes contained internal resonances. This demonstrated that the spikes in RQ-FEP are the result of IRs in the dynamics. In short, the appearance of spikes in the RQ-FEP or similar POMs mean the presence of IRs, while the absence of spikes and dissimilar POMs corresponds to the absence of such IRs.

2 Preliminary Concepts and the Proposed Method

2.1 Proper Orthogonal Decomposition

Proper orthogonal decomposition (POD) [6, 13, 14, 16, 22] is a system identification and model reduction tool that extracts an orthonormal basis of modes, termed the proper orthogonal modes (POMs), that represent a large set of interdependent variables in a least-squares sense. For linear response data, the POMs have been proven to be the minimum number of mutually orthogonal modes necessary to reconstruct that linear response data. Moreover, the POMs converge to the linear normal modes of vibration for classically damped, linear, discrete systems with mass matrices proportional to the identity matrix and in the limit of infinite measurement points [6]. In this work, we consider spatially discretized models of continuous systems obtained using the finite element (FE) method and, accordingly, employ the singular value decomposition (SVD), which is equivalent to POD for discrete systems [6]. The response data matrix X of dimensions $m \times n$ is factored as,

$$X = USV^T, \tag{1}$$

where U is an $m \times m$ orthonormal matrix containing the left singular vectors, S is an $m \times n$ pseudo-diagonal and positive semi-definite matrix containing the singular values, and V is an $n \times n$ orthonormal matrix composed of the right singular vectors. The left singular vectors, which are equivalent to the POMs, and the POVs are computed as the eigenvectors and eigenvalues of the matrix XX^T respectively. The singular values are equal to the POVs squared and divided by the number of samples m. The right singular vectors, V contain the time modulation of the corresponding POMs, normalized by the singular values, and are computed as the eigenvectors of the matrix $X^T X$.

2.2 Rayleigh Quotient

The Rayleigh quotient is a classical operator that uses a trial vector (discrete systems) or function (continuous systems) to estimate the fundamental natural frequency of a linear system. The frequencies of higher vibration modes can be estimated provided that the new trial vector or function is mass-orthogonal to the trial vectors used to estimate the lower modes. Since the FE method is used to discretize the continuous structures in this work, we employ the discrete version of the RQ:

$$R(v) = \frac{v^T K v}{v^T M v}, \tag{2}$$

where v is the trial vector, K is the stiffness matrix, and M is the mass matrix. A celebrated property of the RQ is its relative insensitivity to the trial vector, which permits the use of a large range of trial vectors, provided that the trial vectors satisfy the relevant boundary conditions. Moreover, the RQ has a minimum value equal to the fundamental eigenvalue of the linear mass and stiffness matrices. In this study, the frequencies of each system are estimated using the POMs extracted from the translational degrees of freedom (DOFs) of continuous structures in bending. Although the POMs are not mass-orthogonal (they are mutually orthogonal), we use them independently to estimate the frequencies of their respective modes as

$$f_i = \frac{1}{2\pi}\sqrt{R(v_i)}. \tag{3}$$

Consequently, the procedure is ad hoc and there is no guarantee that the estimated frequencies will correspond to the natural frequencies of the nonlinear systems under study. Nevertheless, it will be shown that the RQ-based procedure will lead to physically meaningful results, indicating that the computed POMs are close to the linear modes of the systems considered.

2.3 The Wavelet-Bounded Empirical Mode Decomposition

The empirical mode decomposition (EMD) proposed by [11] decomposes an oscillatory signal into a finite basis of nearly orthogonal, monochromatic intrinsic mode functions (IMFs). By using a sifting algorithm, EMD decomposes an oscillatory signal, $x(t)$, into N nearly orthogonal IMFs that satisfy

$$x(t) = \sum_{i=1}^{N} c_i(t) + R_{N+1}(t), \qquad \max\left(R_{N+1}(t)\right) < \tau, \tag{4}$$

where $c_i(t)$ is the ith IMF and $R_{N+1}(t)$ is the remainder signal with an amplitude less than the tolerance τ. In theory, each IMF possesses a single characteristic time scale such that the IMF is physically and mathematically representative of a single time scale contained in the original signal [19, 27, 32]. However, in practice, applying EMD often results in more IMFs than the number of characteristic time scales present in the original signal (i.e., the method yields spurious, non-physically meaningful IMFs which need to be eliminated before the dynamical analysis can commence), and care must be taken to select only the physically meaningful IMFs from the extracted ones [10–12].

Another pitfall of EMD is the issue of mode mixing, where a single IMF contains multiple components at different frequencies and, therefore, is not representative of any single time scale contained in the original signal. The wavelet-bounded EMD (WBEMD) [25] solves the issue of mode mixing by isolating each IMF around the frequency of a particular component (NNM). This is accomplished by first applying EMD to the signal combined with a masking signal [3],

$$s(t) = \alpha \max\left[z_i(t)\right] \sin(\beta \omega_i t), \tag{5}$$

where α and β are free parameters used by the optimization routine, ω_i is the frequency of the component being extracted, and

$$z_i(t) = x(t) - \sum_{q=1}^{i-1} c_q(t). \tag{6}$$

Following the application of EMD, the IMF is transformed to the maximum wavelet domain [25], where a bounding function is fitted over the IMF. Finally, the isolation of the IMF is measured by computing the area under the bounding function. It follows that well-separated IMFs result in a bounding-function area that is smaller than that of poorly separated IMFs. Thus, WBEMD minimizes the bounding-function area by adjusting the masking-signal parameters, α and β such that a well-separated IMF is extracted. The use of WBEMD will be critical in the next section, where we will use the IMFs to demonstrate that the proposed method captures these strongly nonlinear interactions while relying only on the systems known linear properties.

2.4 The Proposed Method

The proposed method requires that the system be naturally described by evolving time scales and a characteristic, time-varying energy quantity, that the formulation of the RQ operator be permitted, and that non-mixed response data is available, which reflects the fact that the method is data-driven. By "non-mixed," we mean that all variables or measurements in the response data must possess the same units of measure (i.e., all displacements or accelerations) to ensure that the results from POD are meaningful [2]. Further assumptions are provided in [23]. If the RQ operator cannot be formulated for the system, the method can still be applied using the POMs and their time-varying shapes instead of estimated frequency-energy plots. For mechanical structures undergoing linear and nonlinear vibrations, the modal characteristics of the system and mechanical energy serve as the evolving time scales and characteristic, time-varying energy quantity, respectively. For such systems, the RQ operator is formulated using linear models (FE models in this work) updated to capture the relevant modal properties of the experimental systems. We refer the reader to [5, 8, 28] for discussions of linear model updating. The response data in this work takes the form of displacement response data, which is obtained by numerical integration and filtering of measured acceleration responses.

The proposed method is divided into two processes: first, the nonlinearity is characterized and the accompanying strongly nonlinear modal interactions are identified using the RQ-FEP created using the POMS extracted from the displacement response. Second, the user computes the characteristic displacement (defined below), creates a RQ frequency-displacement plot (RQ-FDP) and identifies the nonlinearity by fitting a model to the RQ-FDP. The method is summarized by the following steps:

1. For n measurement coordinates, extract n POMs using SVD from windowed segments of a single time record.
2. Using the POMs, compute the estimated RQs for the NNMs within the frequency range of interest and plot these as functions of energy or time.
3. Characterize the nonlinearity and identify the modal interactions present in the measured response using the RQ-FEP.
4. Compute the characteristic displacement as defined for the system and plot the RQ estimates as functions of that characteristic displacement to form the RQ-FDP.
5. Based on the previous characterization, propose a model for the nonlinearity and derive the frequency-displacement relationship.
6. dentify the unknown parameters explicitly or using an optimization routine.

The characteristic displacement for the window defined by the interval $[T_1, T_2]$ is

$$\delta_c = \frac{1}{T_2 - T_1} \int_{T_1}^{T_2} |\delta| dt, \tag{7}$$

where δ is the relative displacement between the attachment and the point of attachment on the structure. For discrete signals, the characteristic displacement is defined

as

$$\delta_c = \frac{1}{N}\sum_{n=1}^{N} |\delta_n|, \tag{8}$$

for N points in the interval $[T_1, T_2]$. The resulting characteristic displacement enables us to plot the estimated frequencies as functions of displacement. In this work, we consider a local nonlinear attachment in the form of an NES and model the nonlinearity as $\alpha|\delta|^{\beta}\delta$ where δ is the relative displacement between the NES and its attachment points. For this nonlinearity, the equation of motion for the NES is

$$\ddot{u}_{NES} + \frac{d}{m}\dot{\delta} + \left(\omega_n^2 + \frac{\alpha}{m}|\delta|^{\beta}\right)\delta = 0, \tag{9}$$

and, replacing the relative displacement with the characteristic displacement, the displacement-dependent frequency equation is

$$f(\delta_c) = \frac{1}{2\pi}\sqrt{\omega_n^2 + \frac{\alpha}{m}\delta_c^{\beta}}. \tag{10}$$

As will be seen in Sect. 4, if the estimated frequency of the NES intersects the ith NNM with frequency f_i at the characteristic displacement δ_i, then we can relate α to β by requiring that $f(\delta_i) = f_i$. Thus,

$$\alpha = \frac{m}{\delta_i^{\beta}}\left((2\pi f_i)^2 - \omega_n^2\right), \tag{11}$$

and substituting (11) into (10) results in

$$f(\delta_c) = \frac{1}{2\pi}\sqrt{\omega_n^2 + \left((2\pi f_i)^2 - \omega_n^2\right)\left(\frac{\delta_c}{\delta_i}\right)^{\beta}}. \tag{12}$$

The remaining parameter is identified using an optimization routine (described in [24]) that maximizes the R-squared value between the RQ-FDP for the NES and the model in (12).

3 Detection of Strongly Nonlinear Modal Interactions

The described methodology is validated by being applied to the experimentally measured response of the cantilever shown in Fig. 1a. The beam is low-carbon steel, 0.749 m long with a 0.045×0.008 m^2 cross section and was connected at 0.7 m from its fixed end to two 0.0762 m long steel wires with of diameter 0.0012 m. The wires were attached to a steel shaft extended from the beam via two shaft collars. In

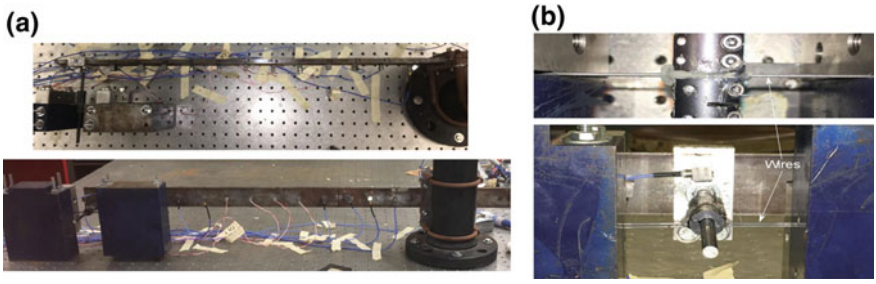

Fig. 1 **a** Top and front view of beam used in experiments. **b** Top and front view of nonlinear attachment. Reprinted with permission from [23]

order to achieve a 3:1 IR with a low-amplitude excitation, the length of the beam and the attachment shown in Fig. 1b were tuned in such a way that the frequency ratio of the two first NNMs was close to 3:1. The beam was excited at the position of the attachment by an impulse from a PCB Piezotronics modal impact hammer (model 086C01). Using PCB accelerometers (models U356A11 and Y353B17) with nominal sensitivities of 1 mV/(m/s2) along with VibPilot hardware (m+p International, Hannover, Germany) and m+p analyzer software, the acceleration responses of 14 locations along the beem were recorded for a duration of 2 s with 16384 Hz sampling rate. Measurements showed that the 9th accelerometer was saturated, and therefore the corresponding data was removed from the data set before analysis. To compute the velocities, the accelerations were numerically integrated and filtered, using a third-order Butterworth high-pass filter with a cutoff frequency of 18 Hz. Numerically integrating the velocities and then high-pass filtering the resulting signal with a cutoff frequency of 10 Hz, the displacements were computed. Additionally, before and after each integration the temporal means of the signals were subtracted so that the accelerations, velocities and displacements had zero mean.

The proposed method is used to study the displacement response of the beam subjected to the large amplitude impact shown in Fig. 2a. The nonstationary nature of the displacement can be seen in both the wavelet and Fourier spectra shown in Fig. 2b. The FFT shows that the first and the second NNMs cover frequency ranges from 21.6 to 31.5 Hz and 68.8 to 73 Hz, respectively, while the third NNM contains only a single peak at 186.6 Hz. Looking at the wavelet spectra of the displacement, the hardening nature of the nonlinearity can be seen; for instance, the first NNM frequency decreases from 31 to 21.5 Hz as the total energy of the system decreases due to dissipation.

Since the method does not require a priori knowledge of the nonlinearity, the nonlinearity was not identified in this work, and the attachment was modeled as a point mass and a discrete linear spring from the beam to ground. For this model, the mass of the attachment was measured to be 0.171 kg and the density of the beam was chosen to be 7800 kg/m3. By matching the first six bending eigenfrequencies of the beam, found from the low-amplitude impact experiment, with those obtained

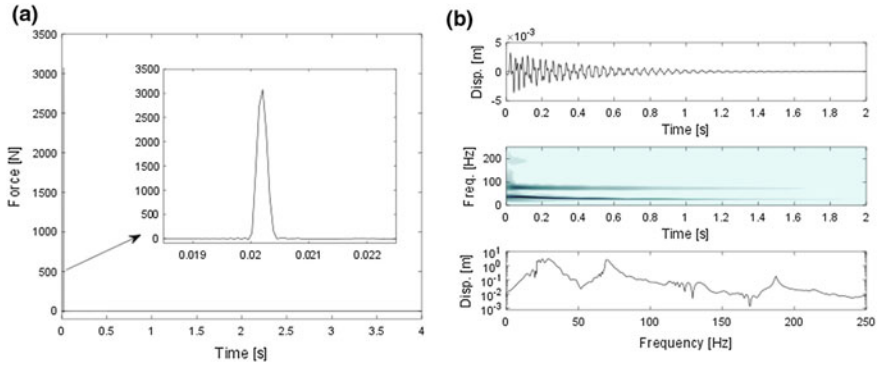

Fig. 2 **a** High-amplitude, impulsive load applied at nonlinearity location, **b** Time series, wavelet transform, and FFT of the displacement at the nonlinearity location (integrated from accelerometer measurements). Reprinted with permission from [23]

from an FE model of the beam using Euler–Bernoulli beam elements, the elastic modulus of the beam and the linear stiffness of the attachment were identified. The GlobalSearch function of MATLAB was used to perform a global minimization of the error norm

$$\varepsilon_k = \sum_{n=1}^{6} \frac{\left|\omega_n^{Exp} - \omega_n^{FE}\right|}{n\omega_n^{Exp}}, \tag{13}$$

where $|\cdot|$ denotes absolute value. The contribution of each mode is weighted by its modal number. Note that by using Guyan reduction method, the rotational DOFs were condensed out of the FE matrices. After performing the global search, the identified values for elastic modulus and linear stiffness turned out to be 1.90×10^{11} N/m^2 and 10854 N/m, respectively, and the average error for the first six bending modes between the experimental and FE model eigenfrequencies was 2.73%.

According to the data presented in Fig. 2b, the energy of the experimental system dissipates quickly within the recorded time window. Thus, in order to capture and analyze the transient response of the experimental system, the 2 s time window needs to be divided into sufficiently small segments to capture at least a half cycle of the first NNM as well as the transient response of the system. Consequently, for the experimental system under study, the 2 s time window is divided into 92 nonoverlapping time segments, each with 0.0216 s duration. Notice that the first 0.0251 s portion of the recorded response is excluded from the data set because this portion was recorded before the impact was applied. Thirteen POMs are extracted out of each time segment. Because of the damping effects, internal resonances are more likely to happen between the first two NNMs than between the higher NNMs, so only the POMs corresponding to the first and second NNMs are taken into consideration. To obtain the final POMs with least effects of measurement noise, a sixth-order polynomial with zero constant, linear and quadratic terms is fitted to each POM at

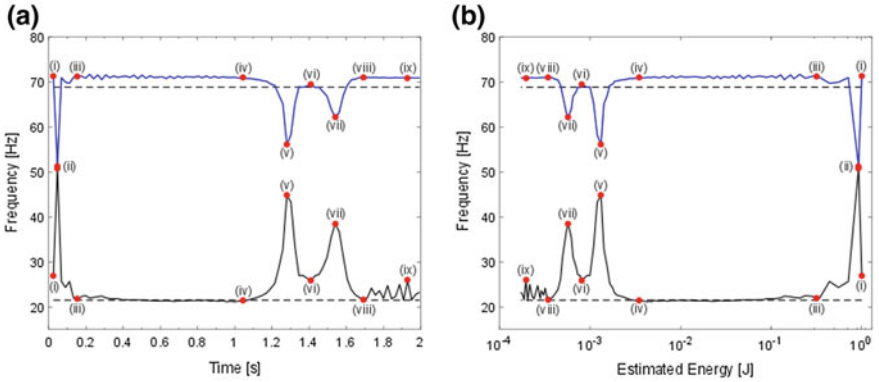

Fig. 3 RQ frequency computed using the POMs corresponding to the first two NNMs plotted as a function of **a** time and **b** estimated energy. The black dashed lines represent the experimental frequencies at low energies. Reprinted with permission from [23]

each accelerometer location. Note that data from the 9th accelerometer was not used because of the reason explained before.

That the first capture happens in such a short period of time implies that a great amount of energy is dissipated quickly, which is not caused only by the viscous damping in the system. The other factor that causes this rapid dissipation of energy is the IR that is indicated by the first spike in Fig. 3a, b. During this modal interaction, the energy in the first NNM is irreversibly transferred to the second NNM, and there it gets dissipated at a higher rate. Looking at the wavelet spectrum of the system during the first spike, i.e. Fig. 3b, one can see that the frequency ratio of the second and first NNMs is 72 to 28.6 Hz, which is approximately a 5:2 ratio. This ratio indicates that first spike is the result of a 5:2 IR.

While the first spike in the RQ happens in a short period of time, the second and third spikes occur for a longer period of time and almost right after each other. These two spikes being close to each other indicates that the third IR happens almost immediately after the second IR, which corresponds to the second spike. According to the wavelet spectrum shown in Fig. 2b, the frequencies of the first and second NNMs during these IRs are 23 and 68.8 Hz, respectively, which indicate 3:1 IRs during the second and third spikes. It should be mentioned that the system was tuned so that a 3:1 IR can be achieved at low energy levels, which explains why the last two IRs remain active for a longer period of time compared to the first spike. Moreover, because of this tuning, for a certain change in the energy level of the system, the frequency change around the 3:1 IR is much lower than that around the 5:2 IR. For this reason, it can be concluded that the energy threshold for 3:1 IR to happen is much larger than the threshold for a 5:2 IR to happen. Several spikes with small amplitude on the curve for the first spike can be seen from 1.7 to 2 s, which one may consider as modal interactions. Because the first POM corresponding to these spikes corresponds to only the first NNM (specifically, the only node is at the

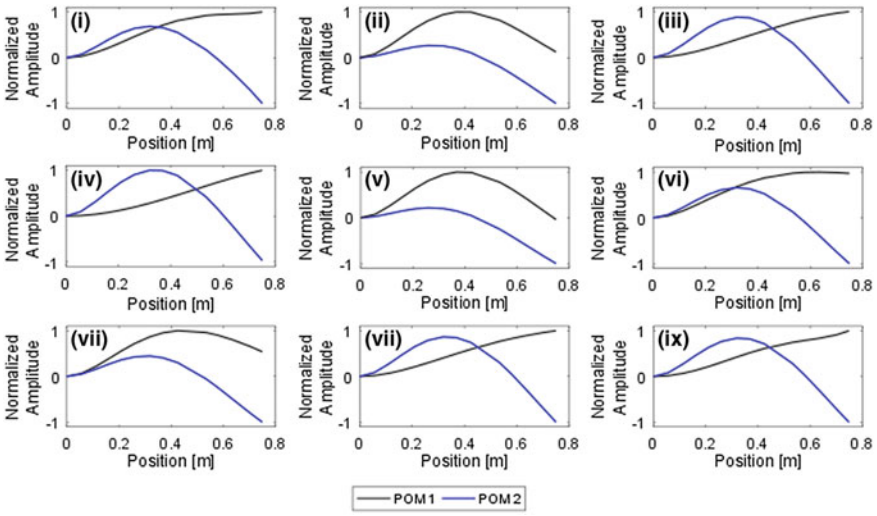

Fig. 4 POMs 1 and 2 for each of the nine red dots in Fig. 3. Reprinted with permission from [23]

fixed boundary), we can conclude that these spikes are results of signal decay, small measurement and numerical errors.

The POMs corresponding to the nine red dots in Fig. 3 are shown in Fig. 4. While away from the spikes, i.e. at points i, iii, iv, vi, viii, and ix, the POMs represent the periodic solutions of their corresponding NNMs. However, on the spikes, i.e. at points ii, v, and vii, the POMs become similar to the periodic solution of the second NNM, in which both POMs have one anti-node near the center and one at the free end. These results are very similar to those obtained for the computational system, which is further evidence that the previous theoretical results represent physical phenomena. Also, in accordance to what was explained before, one can clearly see that the POMs corresponding to the first and second NNMs are not similar on spike ix. This means that even though there is a spike on point ix, but this spike does not represent any modal interactions between the first and second NNMs. Additionally, the slight oscillation that has appeared in the first POM is caused by small measurement and numerical errors that result in deviation from the linear, experimental natural frequency.

The existence of IRs is demonstrated by computing the slow phases of the NNMs. Up to this point, WBEMD is applied to the response presented in Fig. 2b, four well-separated IMFs which represent four individual NNMs are extracted and their corresponding phase trajectories are computed. Since it was predicted that the first modal interaction corresponds to a 5:2 IR, the corresponding phase trajectory, along with a zoomed-in view of its initial portion, is plotted in Fig. 5a. The single loop in the zoomed-in view occurs between 0.02 and 0.13 s, which is the duration of the first spike shown in Fig. 3. The presence of this loop and its correspondence with the first spike is a further proof that the first spike is indeed the result of a 5:2 IR and not a

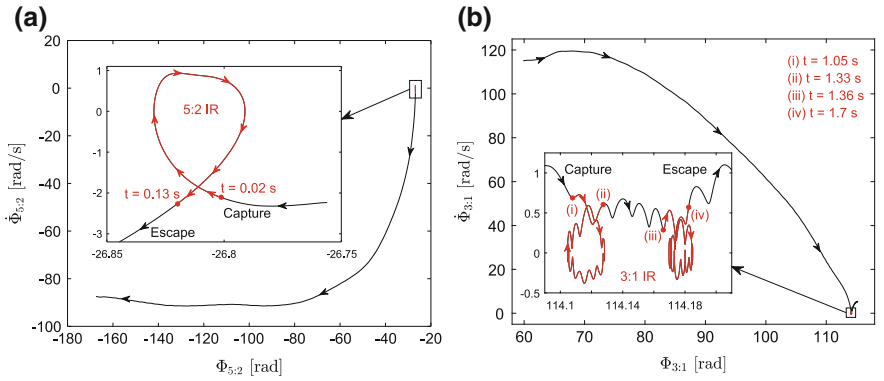

Fig. 5 **a** Phase trajectory for $\Phi_{5:2}(t) = 5\theta_1(t) - 2\theta_2(t)$, which corresponds to the second and third spikes in Fig. 3. **b** Phase trajectory for $\Phi_{3:1}(t) = 3\theta_1(t) - 1\theta_2(t)$, which corresponds to the first spike in Fig. 3. Reprinted with permission from [23]

numerical artifact. Figure 5b and its zommed-in views depict 3:1 trajectories and the two loops corresponding to the second and third spikes, respectively. These loops are non-time-like and indicate that 3:1 IRs occur between the first and second NNMs. As before, the interval in which each loop occurs corresponds to the duration of the loops corresponding spikes. Moreover, the fact that there are two loops in the 3:1 trajectory plot confirms the modal interactions represented as spikes in Fig. 3.

According to the presented and discussed results, the current method proves to be a valuable and powerful tool for detecting strongly nonlinear modal interactions directly from measured data. By means of this method one can get significant insight into the governing nonlinear physics of the response of dynamical systems with smooth and local nonlinearities. Hence, this method is a valuable tool to gain a thorough understanding of the transient responses of strongly nonlinear dynamical systems, including nonlinear modal interactions caused by IRs.

4 Nonlinear System Identification of a Strongly Nonlinear Attachment

To demonstrate the NSI procedure presented in Sect. 2.4, we apply it to the experimentally measured response of the cantilevered wing in Fig. 6a. The wing is aluminum and detailed dimensions can be found in [24]. A local NES is attached to the free end of the wing. The nonlinearity is realized through transverse displacements of thin steel wires, which are fixed at both ends and each have a diameter of 0.00036 m and a length of 0.0552 m. The attachment, depicted in Fig. 6b, results in a hardening-type, ideally essential nonlinearity; however, the resulting force-displacement relationship is not purely nonlinear. Instead, a small linear stiffness is introduced by pretension in

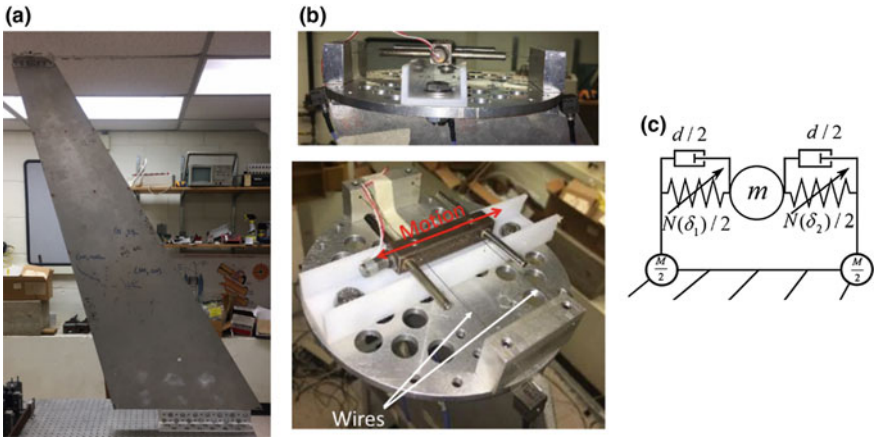

Fig. 6 **a** Front view of wing used in experiments. **b** Front and top view of the nonlinear attachment. **c** Model used for the nonlinear attachment and baseplate. Modified and reprinted from [24]

the wires due to the boundary conditions, resulting in a natural frequency associated with the motion of the NES. The diameter of the wires was tuned such that a 1:1 IR between the NES and the second NNM is realizable using a standard modal hammer. The acceleration responses of the wing and the NES were measured using PCB Piezotronics accelerometers (models U356A11 and Y353B17) for an impact applied using a PCB Piezotronics modal impact hammer (model 086C01). The acceleration response of the wing was measured at 14 location along the leading and trailing edges. Using VibPilot hardware (m+p International, Hannover, Germany) and m+p analyzer software, the responses were measured for a duration of 8 s at a sampling rate of 4096 Hz. The displacement and velocity responses of the wing and NES were obtained using the same numerical integration scheme used in the prior experiments with the cantilever beam, except that the cut-off frequency was set to 2 Hz.

To demonstrate the proposed NSI method, we study the response of the wing to the impact depicted in Fig. 7a. The corresponding velocity response of the NES and the corresponding wavelet transform and frequency response function (FRF) are depicted in Fig. 7b. Both the wavelet and FRF reveal the nonstationary nature of the response. Full details of the model for the wing and NES are provided in [24]; we present a summary of the modeling procedure here. The wing is modeled using the FE mesh described in [24] using an elastic modulus of N/m2 and a density of 2700 kg/m^3. The added mass of the base plate is modeled as two lumped masses at the leading and trailing edges of the free end of the wing, which allows the added mass to affect both the bending and torsional NNMs. The mass of the base plate was measured to be 0.408 kg. The attachment is modeled as a discrete mass with linear and nonlinear springs coupling it to the leading and trailing edges. The mass of the attachment is found to be 0.908 kg, and the frequency of the NES at small energy is 8.36 Hz. The linear stiffness coupling the NES to the wing was computed to be 241.5

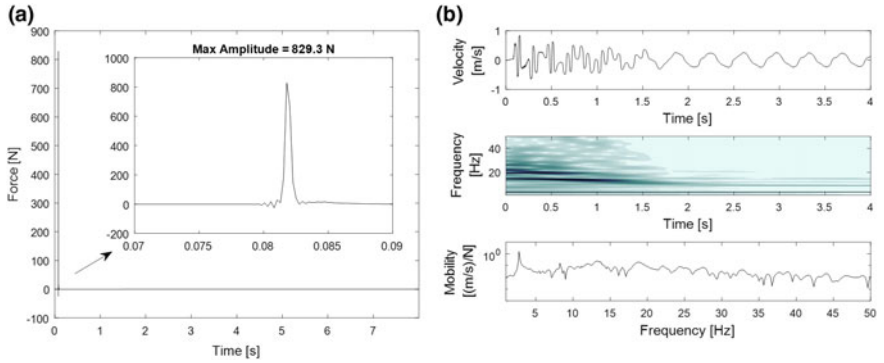

Fig. 7 **a** High-amplitude, impulsive load applied at nonlinearity location, **b** Time series, wavelet transform, and FRF of the velocity of the NES (integrated from accelerometer measurements). Reprinted from [24]

N/m using an optimization routine that minimized the error between the frequency of the NES NNM in the FE model and that of experimental system.

As in Sect. 3, the time window is divided into segments that are sufficiently small to capture the transient nature of the response, but large enough to capture at least one-half cycle of the first NNM. For this system, we use a segment length of 0.173 s and consider the response in the window defined by [0.09,7.5], which results in a total of 42 nonoverlapping time segments. The first 0.09 s of the measurement is excluded from the analysis because it contained the response of the wing to ambient vibration before the impact. For each time segment, we extract 15 POMs; however, only those corresponding to the first four NNMs are analyzed. A fourth-order polynomial with no constant or linear terms is fitted to each POM, which reduces the effect of measurement noise. The final POMs are created by evaluating the polynomials at each accelerometer location.

Using the POMs, we compute the RQ for the first four NNMs for each time segment and plot them as functions of time in Fig. 8a. In this plot, there are two periods of IR between the NES and the second NNM. The first occurs from an energy of 0.363–0.103 J and the second corresponds to the spike that occurs at 0.0880 J. For this system, the relative displacement is defined as the difference between the displacement of the NES and the average of the displacement of the leading and trailing edges at the tip of the wing. Following the procedure presented in Sect. 2.4, we compute the characteristic displacement defined by (8) for each segment and plot the RQ in Fig. 8b, where the frequency-displacement pairs have been sorted in ascending order based on the displacements. Using the low-energy frequency of the second NNM, $f_2 = 14.34$ Hz, the corresponding characteristic displacement is found to be $\delta_2 = 0.00150$ m using linear interpolation. Using the optimization routine described in [24], the parameters $\alpha = 3.4887 \times 10^8$ N/m$^{3.0714}$ and $\beta = 2.0714$ are found. The resulting frequency-displacement curve for the identified parameters is depicted as the red line in Fig. 8b.

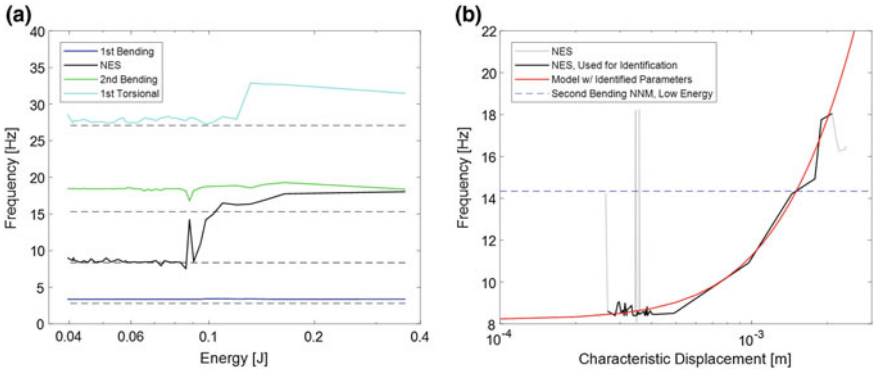

Fig. 8 **a** The RQ-FEP for the response depicted in Fig. 7. **b** Comparison of the RQ FDP for the NES and the identified model. Modified and reprinted from [24]

The identified model is validated by comparing its response to that of the exact system for multiple forcing values. Although the nonlinearity is identified using displacements, the displacement response is dominated by the first bending mode (which is why this NNM was filtered out from the characteristic displacement), and effects from higher NNMs are difficult to ascertain. Instead, we present the velocity responses of the measured and identified systems in Fig. 9a for the impact depicted in Fig. 7a, which corresponds to the response used to perform the identification. The velocity responses for impacts of 264.8, 504.4 and 1158.6 N are shown in Fig. 9b–d, respectively, and correspond to measurements that were not used to perform the identification. The match between the velocity responses, the wavelets and the FRFs confirm that the identified system accurately models the measured system for multiple forcing impacts. These results validate the proposed method for nonlinear system identification of strongly nonlinear attachments in both theoretical and experimental frameworks.

5 Concluding Remarks

We studied the experimental responses of two mechanical systems with smooth, local nonlinearities. The first system was a cantilever beam with a smooth, nonlinear spring attached near its free end and the second system was a model airplane wing with a local NES connected to the tip. Using POD, energy-dependent POMs were extracted from the displacement responses of each system, and were representative of the NNMs governing each system. For both systems, the frequencies of the NNMs were estimated using the discrete RQ with the POMs as trial vectors. The estimated frequencies were plotted as functions of time and energy, which revealed the presence of non-smooth perturbations (spikes), which appeared to indicate strongly nonlinear

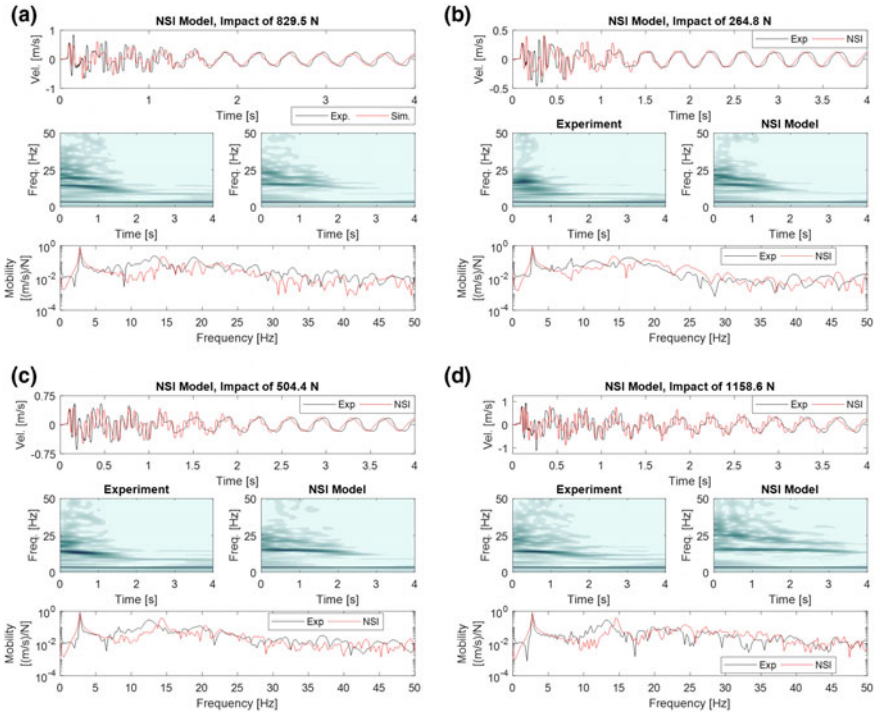

Fig. 9 The measured and predicted response for impacts of **a** 829 N, **b** 265 N, **c** 504 N and **d** 1158 N. Modified and reprinted from [24]

modal interactions. The POMs corresponding to the points off and on the spikes were found to be similar to the periodic solutions of non-interacting and interacting NNMs, respectively.

The displacement response of the beam was decomposed into well-separated IMFs using WBEMD, and using the Hilbert transform a phase variable for each spike was defined and the corresponding phase trajectories examined. The spikes were found to correspond to periods of non-time-like behavior (loops), which indicated the presence of strongly nonlinear IRs. The estimated frequencies of the model wing were also plotted as functions of characteristic displacement, which was used to identify the nonlinear stiffness coupling the NES to the wing. The resulting model accurately reproduced the relevant nonlinear dynamics for all four loading cases investigated.

Funding. This material is based upon work supported in part by the National Science Foundation Graduate Research Fellowship under Grant No. DGE-1144245.

Disclaimer. Any opinion, findings, and conclusions or recommendations expressed in this material are those of the authors(s) and do not necessarily reflect the views of the National Science Foundation.

References

1. Attar, M., Karrech, A., Regenauer-Lieb, K.: Non-linear modal analysis of structural components subjected to unilateral constraints. J. Sound Vib. **389**, 380–410 (2017). https://doi.org/10.1016/j.jsv.2016.11.012
2. Chatterjee, A.: An introduction to the proper orthogonal decomposition. Curr. Sci. **78**(7), 808–817 (2000)
3. Deering, R., Kaiser, J.: The use of a masking signal to improve empirical mode decomposition. In: IEEE International Conference on Acoustics, Speech, and Signal Processing (ICASSP '05), vol. 4, pp. 485–488. (2005). https://doi.org/10.1109/ICASSP.2005.1416051
4. Ehrhardt, D.A., Allen, M.S., Beberniss, T.J., Neild, S.A.: Finite element model calibration of a nonlinear perforated plate. J. Sound Vib. **392**, 280–294 (2017). https://doi.org/10.1016/j.jsv.2016.12.037
5. Ewins, D.J.: Modal Testing: Theory, Practice, and Application. Research Studies Press, Philadelphia (2000)
6. Feeny, B.F., Kappagantu, R.: On the physical interpretation of proper orthogonal modes in vibrations. J. Sound Vib. **211**(4), 607–616 (1998). https://doi.org/10.1006/jsvi.1997.1386
7. Flandrin, P., Rilling, G., Goncalves, P.: Empirical mode decomposition as a filter bank. IEEE Signal Process. Lett. **11**(2), 112–114 (2004). https://doi.org/10.1109/LSP.2003.821662
8. Friswell, M.I., Mottershead, J.E.: Finite Element Model Updating in Structural Dynamics. Springer Science and Business Media, Berlin (1995)
9. Herrera, C.A., McFarland, D.M., Bergman, L.A., Vakakis, A.F.: Methodology for nonlinear quantification of a flexible beam with a local, strong nonlinearity. J. Sound Vib. **388**, 298–314 (2017). https://doi.org/10.1016/j.jsv.2016.10.037
10. Huang, N., Wu, M.L., Long, S., Shen, S., Qu, W., Gloersen, P., Fan, K.: A confidence limit for the empirical mode decomposition and Hilbert spectral analysis. Proc. Royal Soc. A: Math. Phys. Eng. Sci. **459**(2037), 2317–2345 (2003). https://doi.org/10.1098/rspa.2003.1123
11. Huang, N.E., Shen, Z., Long, S.R., Wu, M.C., Shih, H.H., Zheng, Q., Yen, N.C., Tung, C.C., Liu, H.H.: The empirical mode decomposition and the Hilbert spectrum for nonlinear and non-stationary time series analysis. Proc. Royal Soc. A: Math. Phys. Eng. Sci. **454**(1971), 903–995 (1998)
12. Huang, N.E., Shen, Z., Long, S.R.: A new view of nonlinear water waves: the Hilbert spectrum 1. Annu. Rev. Fluid Mech. **31**(1), 417–457 (1999). https://doi.org/10.1146/annurev.fluid.31.1.417
13. Karhunen, K.: Uber lineare methoden in der wahrscheinlichkeitsrechnung, (1947)
14. Kerschen, G., Golinval, J.C., Vakakis, A., Bergman, L.: The method of proper orthogonal decomposition for dynamical characterization and order reduction of mechanical systems: an overview. Nonlinear Dyn. **41**(1–3), 147–169 (2005). https://doi.org/10.1007/s11071-005-2803-2
15. Kerschen, G., Worden, K., Vakakis, A.F., Golinval, J.C.: Past, present and future of nonlinear system identification in structural dynamics. Mech. Syst. Signal Process. **20**(3), 505–592 (2006). https://doi.org/10.1016/j.ymssp.2005.04.008
16. Kosambi, D.: Statistics in function space. J. Indian Math. Soc. **7**(1), 76–88 (1943)
17. Kurt, M., Eriten, M., McFarland, D.M., Bergman, L.A., Vakakis, A.F.: Strongly nonlinear beats in the dynamics of an elastic system with a strong local stiffness nonlinearity: analysis and identification. J. Sound Vib. **333**(7), 2054–2072 (2014). https://doi.org/10.1016/j.jsv.2013.11.021
18. Lee, Y., Nucera, F., Vakakis, A., McFarland, D., Bergman, L.: Periodic orbits, damped transitions and targeted energy transfers in oscillators with vibro-impact attachments. Phys. D: Nonlinear Phenom. **238**(18), 1868–1896 (2009). https://doi.org/10.1016/j.physd.2009.06.013
19. Lee, Y.S., Tsakirtzis, S., Vakakis, A.F., Bergman, L.A., McFarland, D.M.: Physics-based foundation for empirical mode decomposition. AIAA J. **47**(12), 2938–2963 (2009). https://doi.org/10.2514/1.43207

20. Lee, Y.S., Vakakis, A.F., McFarland, D.M., Bergman, L.A.: A global-local approach to nonlinear system identification: a review. Struct. Control Health Monit. **17**(7), 742–760 (2010). https://doi.org/10.1002/stc.414
21. Lee, Y.S., Tsakirtzis, S., Vakakis, A.F., Bergman, L.A., McFarland, D.M.: A time-domain nonlinear system identification method based on multiscale dynamic partitions. Meccanica **46**(4), 625–649 (2011). https://doi.org/10.1007/s11012-010-9327-7
22. Lévy, P., Loève, M.: Processus stochastiques et mouvement brownien. Gauthier-Villars, Paris (1948)
23. Moore, K.J., Kurt, M., Eriten, M., McFarland, D.M., Bergman, L.A., Vakakis, A.F.: Direct detection of nonlinear modal interactions from time series measurements. Mech. Syst. Signal Process. (2018). https://doi.org/10.1016/j.ymssp.2017.09.010. (in press)
24. Moore, K.J., Kurt, M., Eriten, M., McFarland, D.M., Bergman, L.A., Vakakis, A.F.: Data-driven system identification of strongly nonlinear attachments, (2018). (in preparation)
25. Moore, K.J., Kurt, M., Eriten, M., McFarland, D.M., Bergman, L.A., Vakakis, A.F.: Wavelet-bounded empirical mode decomposition for measured time series analysis. Mech. Syst. Signal Process. **99**, 14–29 (2018)
26. Noël, J.P., Kerschen, G.: Nonlinear system identification in structural dynamics: 10 more years of progress. Mech. Syst. Signal Process. **83**, 2–35 (2017). https://doi.org/10.1016/j.ymssp.2016.07.020
27. Sharpley, R.C., Vatchev, V.: Analysis of the intrinsic mode functions. Constr. Approx. **24**(1), 17–47 (2005). https://doi.org/10.1007/s00365-005-0603-z
28. Silva, J.M.M.: Modal Analysis and Testing. Springer, Netherlands, Dordrecht (1999)
29. Vakakis, A., Gendelman, O., Bergman, L., McFarland, D., Kerschen, G., Lee, Y.: Nonlinear targeted energy transfer in mechanical and structural systems I. Solid Mech. Appl. **156**, 1–1033 (2008)
30. Vakakis, A.F., Manevitch, L.I., Mikhlin, Y.V., Pilipchuk, V.N., Zevin, A.: Normal Modes and Localization of Nonlinear Systems. Wiley, New York (1996)
31. Vakakis, A.F., Bergman, L.A., McFarland, D.M., Lee, Y.S., Kurt, M.: Current efforts towards a non-linear system identification methodology of broad applicability. Proc. Inst. Mech. Eng. Part C: J. Mech. Eng. Sci. **225**(11), 2497–2515 (2011). https://doi.org/10.1177/0954406211417217
32. Vatchev, V., Sharpley, R.: Decomposition of functions into pairs of intrinsic mode functions. Proc. R. Soc. A: Math. Phys. Eng. Sci. **464**(2097), 2265–2280 (2008)
33. Wu, Z., Huang, N.E.: Ensemble empirical mode decomposition: a noise-assisted data analysis method. Adv. Adapt. Data Anal. **01**(01), 1–41 (2009). https://doi.org/10.1142/S1793536909000047